Numerical Study of Scalar Mixing in Curved Channels at Low Reynolds Numbers

S. P. Vanka, G. Luo, and C. M. Winkler
Dept. of Mechanical and Industrial Engineering, University of Illinois at Urbana–Champaign, Urbana, IL 61801

DOI 10.1002/aic.10196
Published online in Wiley InterScience (www.interscience.wiley.com).

A computational study has been performed to determine the rates of mixing in a curved square duct at low Reynolds numbers of interest to microfluidic applications. Two flow streams with inlet scalar concentrations of zero and unity in the two halves of a duct perpendicular to the plane of curvature were allowed to mix by convection and diffusion. Concentration distributions and unmixedness coefficients are presented for several Reynolds and Schmidt numbers and are compared with values for a straight channel of equivalent length. It is seen that for large Schmidt number fluids, mixing is considerably enhanced at moderately low Reynolds numbers (Re ~ 10), but is not enhanced at Reynolds numbers of the order of 0.1. © 2004 American Institute of Chemical Engineers *AIChE J,* 50: 2359–2368, 2004
Keywords: scalar mixing, curved channels

Introduction

Rapid mixing of two (or several) streams is essential to many microfluidic devices currently under development (Brody et al., 1996; Gravesen et al., 1993; Jensen, 2001). In these devices, two (or many) streams of fluid enter a chamber (or a channel), mix, and may undergo a chemical reaction. The fluids to be mixed are usually liquids with small diffusion coefficients (Schmidt numbers of the order of 1000 or greater). Also the characteristic dimension of these channels can be of the order of a few hundreds of microns. For the chosen volumetric rates of the flow, the Reynolds numbers encountered are very small, ranging anywhere from 0.1 to 50. Because of such low Reynolds numbers and high Schmidt numbers, mixing in these devices is slow, dictated primarily by the laminar diffusion coefficient. The molecular diffusion-based mixing time can be expressed as

$$\text{time} \propto \frac{L^2}{\alpha} \tag{1}$$

where L is a characteristic length scale of the mixer (commonly a channel width) and α is the scalar diffusivity. For systems that have dimensions on the order of tens of microns, the molecular diffusion-based mixing time is on the order of seconds. For other mixers with dimensions on the order of hundreds of microns, molecular diffusion-based time for complete mixing can be tens of seconds. These diffusion times are large and thus several innovative methods (Branebjerg et al., 1996; Deshmukh et al., 2000; Evans et al. 1997; Lee et al., 2000, 2001; Liu et al., 2000; Miyake et al., 1993; Volpert et al., 1999; Yi and Bau, 2000; Yi et al., 2000) have been proposed in the past to enhance mixing over the purely diffusive limit.

The numerous mixer designs previously proposed can be classified in two main categories: active and passive. Active mixers use features such as moving walls, bubbles, or pulsed pressure gradients and pulsed flows to enhance mixing. Evans et al. (1997) developed a mixer based on chaotic advection principles (Aref, 1984; Jones et al. 1989). It consisted of two antisymmetric source/sink combinations that were pulsed at a certain frequency. A mixing chamber was filled with two fluid layers one on top of the other. The source and sink dipole was then pulsed for 18 cycles, which resulted in one fluid penetrating and mixing with the other. The flow unsteadiness was generated using bubble pumps. Deshmukh et al. (2000) used alternate pulsing of two streams in a straight channel to mix the two fluids. The pulsing was achieved by alternately generating

Correspondence concerning this article should be addressed to S. P. Vanka at spvank@uiuc.edu.

and collapsing a bubble, which pushed the fluid through a one-way check valve. Volpert et al. (1999) also based their design on chaotic advection. In their design a time-dependent flow was induced by secondary channels that were connected transversely to a main mixing channel. Lee et al. (2000) also used active pulsing of the flow to generate chaotic distortions in the flow field, which aided mixing. Two syringe pumps in conjunction with two solenoids were used to actively control the flow in the mixer. With no external perturbations, little mixing took place in the channel. However, mixing was seen to improve considerably when the flow was pulsed with a period of 1.8 s. Lee et al. (2001) built a micromixer in which the streamlined flow was perturbed by two opposed pressure perturbations. Also considered in this paper was a mixer in which a time-varying electrophoretic force was applied to the two streams. The motion of one fluid by the applied electrical field entrained one into the other. Yi et al. (2000) proposed a peristaltic mixer consisting of a wavy channel with a deformable wavy surface. The wavy surface was deformed with a periodic perturbation, giving a peristaltic motion to the fluid. The advection of the particles, attributed to the oscillating boundary, provided enhanced mixing.

Although some active mixers produce excellent mixing, they are often difficult to fabricate and maintain. In addition, certain biological species may be damaged by the induced heating. Passive mixers are attractive because of their ease of operation and manufacturing. Several passive mixer geometries have been previously proposed (Branebjerg et al., 1996; Liu et al., 2000; Miyake et al., 1993; Yi and Bau, 2000). Because diffusion is the main mechanism available at low Reynolds numbers, it can be increased only by increasing the interface area or by decreasing the distance over which diffusion takes place. A common technique proposed in previous works has been lamination (Branebjerg et al., 1996), in which the two streams are split into several thin alternate layers of the two fluids. Thus, not only the surface area is increased, but the diffusion distance is also decreased. In an effort to increase the diffusion surface area, Miyake et al. (1993) constructed microplumes through a large number of micronozzles. The nozzles were spaced 100 μm apart, and 400 microplumes were generated. The plumes entrained the surrounding fluid while providing enhanced surface area. However, the shear induced by the flow expansions can damage certain molecules. Bend-induced stirring is another way to enhance mixing. When the flow turns a right-angled bend, secondary vortices are generated. These vortices advect fluid from one region to the other, producing mixing. However, at low Reynolds numbers, the vortices decay very fast because of viscous action. Hence several bends must be used to repeatedly produce these secondary flows. Because these vortices decay, and the flow becomes one-dimensional in straight sections, the so-called chaotic advection is not produced. Hence, Liu et al. (2000) fabricated an interconnect of three-dimensional bends, which created a flow field that led to chaotic advection. Experiments were conducted at high Reynolds numbers (up to 70). Results of their tests indicate that such a mixer produced much better mixing than a series of two-dimensional bends and a straight channel. Confirmation of these same phenomena was reported by Yi and Bau (2000), who also studied bend-induced stirring. They confirmed that at low Reynolds numbers, the bend-induced vortices quickly dissipated after the bend.

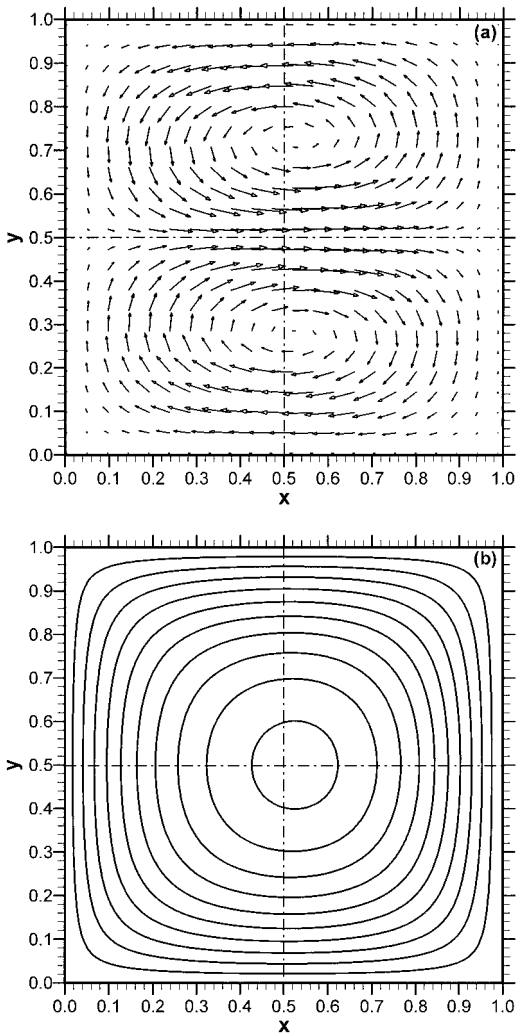

Figure 1. Typical secondary flow pattern (a) and contours of axial velocity in the duct cross section (b).

Present Configuration

The mixer configuration considered herein relies on a *sustained* presence of curvature-induced secondary flows. In contrast to the designs of Liu et al. (2000) and Yi and Bau (2000), in which the stirring of the two fluids was produced by a series of short rectangular bends, the present configuration uses a continuous curvature to sustain the secondary flows. The bend-induced cross-stream vortices generated in these two cited works were observed to decay quickly in the downstream straight sections of the bend because of the viscous effects. Hence, the mixing enhancement was not substantial. The three-dimensional network of bends produced better mixing than a single bend, but the fabrication of such mixers is cumbersome. Here we consider a curved duct that may be wound either with a constant radius or as a spiral.

The flow field in a curved duct has been well studied (Berger et al., 1983; Dean, 1927;Ghia and Sokhey, 1977; Pratap and Spalding, 1975; Thangam and Hur, 1990). When a fluid flows through a curved duct, secondary flows are generated in the cross-sectional plane of the channel (Figure 1). These second-

ary flows (known as Dean's vortices) are a result of differential centrifugal forces acting on the fluid at the center and at the near-wall regions of the duct. In the center of the duct the axial (streamwise) velocities are greater than those near the walls. Therefore the fluid in the center is pushed to the outside of the bend with a force greater than that at the walls. Fluid in the center is driven to the outside of the bend, and by the continuity constraint, it returns along the walls to the inside of the bend. A radial pressure gradient is set up to balance the curvature-induced centrifugal force. The axial velocity profile is distorted from that of a straight duct with the peak shifted to the outside of the bend. The nondimensional parameter characterizing flow in curved ducts is the Dean number De, defined as De = $\mathrm{Re}\sqrt{d/R}$, where Re is the Reynolds number ($\bar{u}d/\nu$), $\bar{u}$ is the average streamwise velocity, d is the width of the channel, ν is the kinematic viscosity, and R is the radius of curvature. As the Dean number increases, so does the intensity of the secondary flow. Dean vortices are generated at any finite Dean number, and thus even a persistent, small secondary flow can generate a complex advection sufficient to mix two fluid streams efficiently. The study of secondary flows can be traced back to very early research in fluid mechanics. A review of some of these works is available in Berger et al. (1983). In all these studies, the magnitude of the secondary flows, and the enhanced shear stress and heat transfer rates have been the quantities of primary interest. However, to our knowledge, no previous studies have used the benefit of these sustained Dean vortices to enhance mixing at low Reynolds numbers encountered in microfluidic channels. Herein, we have performed a number of numerical computations to study the extent of mixing produced by duct curvature. The study is limited to low Reynolds numbers characteristic of micromixers and microcombustors.

Governing Equations and Numerical Procedure

Given that the Reynolds numbers considered here were small, we assumed that the flow became fully developed immediately after it entered the curved channel. For a straight square duct the hydrodynamic entry length (z/d) is approximately 0.1 times the Reynolds number. This is quite small even at the upper limit of the currently considered Reynolds numbers. Because the mixing distances considered were about 60 diameters, the hydrodynamic developing length is small compared to the mixing distance. As a result, we needed to solve only the equations for a fully developed flow in a curved duct. However, the scalar field is three-dimensional (3-D) because the concentration varied in the cross-stream and along the duct length. Because the scalar diffusivity is taken to be small, the Peclet number [Reynolds number times the Schmidt number ($\mathrm{Re}\cdot\mathrm{Sc}$)] in the streamwise direction is large. Thus the streamwise diffusion can be neglected compared to advection. However, the cross-stream Peclet numbers are small, and thus diffusion in these directions was retained. This considerably reduced the computational burden from that of a fully 3-D calculation.

We first determined the fully developed velocity field for a curved square duct by a fully elliptic 2-D calculation. This flow field with three nonzero velocity components was then used to march a parabolized scalar transport equation. Hence the scalar field was stored for only one cross-sectional plane. The scalar transport equation was solved by marching in the streamwise direction from the entrance to the exit of the channel. In the following section, we give details of the governing equations, the numerical procedure, and the details of the computations. This is followed by a section on discussion of the results.

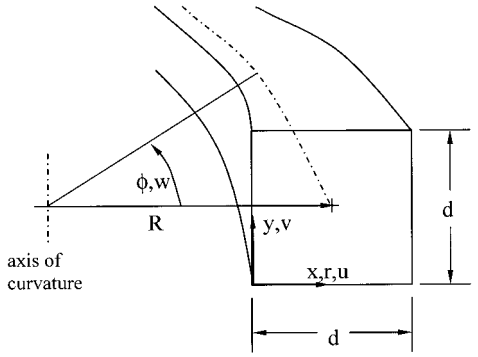

Figure 2. Coordinate system used for the computations.

For the coordinate system and velocity nomenclature shown in Figure 2, the equations for a constant density, constant viscosity fluid may be stated as

Mass Continuity

$$\frac{\partial v}{\partial y}+\frac{1}{r}\frac{\partial (ru)}{\partial r}=0 \tag{2}$$

r-Momentum

$$\frac{1}{r}\frac{\partial}{\partial r}(ruu)+\frac{\partial}{\partial y}(vu)-\frac{w^2}{r} = -\frac{1}{\rho}\frac{\partial p}{\partial r}+\nu\left[\frac{1}{r}\frac{\partial}{\partial r}\left(r\frac{\partial u}{\partial r}\right)+\frac{\partial^2 u}{\partial y^2}-\frac{u}{r^2}\right] \tag{3}$$

y-Momentum

$$\frac{1}{r}\frac{\partial}{\partial r}(ruv)+\frac{\partial}{\partial y}(vv)=-\frac{1}{\rho}\frac{\partial p}{\partial y}+\nu\left[\frac{1}{r}\frac{\partial}{\partial r}\left(r\frac{\partial v}{\partial r}\right)+\frac{\partial^2 v}{\partial y^2}\right] \tag{4}$$

ϕ-Momentum

$$\frac{1}{r}\frac{\partial}{\partial r}(ruw)+\frac{\partial}{\partial y}(vw)+\frac{uw}{r} = -\frac{1}{\rho r}\frac{\partial p}{\partial \phi}+\nu\left[\frac{1}{r}\frac{\partial}{\partial r}\left(r\frac{\partial w}{\partial r}\right)+\frac{\partial^2 w}{\partial y^2}-\frac{w}{r^2}\right] \tag{5}$$

Passive Scalar

$$\frac{1}{r}\frac{\partial}{\partial r}(ruc)+\frac{\partial}{\partial y}(vc)+\frac{\partial}{r\partial \phi}(wc)=\frac{\nu}{\mathrm{Sc}}\left[\frac{1}{r}\frac{\partial}{\partial r}\left(r\frac{\partial c}{\partial r}\right)+\frac{\partial^2 c}{\partial y^2}\right] \tag{6}$$

Here u and v are the nondimensional velocities in the r and y directions, respectively; w is the nondimensional velocity in the streamwise (ϕ) direction; p is the nondimensional pressure; c is the scalar mass fraction; and Sc is the Schmidt number. Note that, because the flow was fully developed, $\partial p/r\partial\phi$ will be constant in the w-momentum equation. ρ and ν are the density and kinematic viscosities, respectively. The radius r is measured from the axis of curvature (Figure 2). Note that the streamwise gradients of velocity are zero. The streamwise diffusion of concentration was neglected, but the streamwise advection term was nonzero. The cross-stream diffusion and advection by the secondary flow are fully included.

The boundary conditions for the equations were no-slip conditions on the solid walls for the velocities, and zero-derivative conditions for the scalars. For the streamwise momentum equation, the streamwise pressure gradient was iteratively adjusted such that the desired Reynolds number was obtained. At the inlet, concentrations of 0 and 1 were prescribed in the halves of the duct perpendicular to the plane of curvature. The initial concentration was such that the interface was perpendicular to the direction of the secondary flow. The flow field was first solved because the scalar field did not influence the values of density and viscosity. A finite-volume procedure with staggered location of velocities and pressures was used to discretize the equations (Patankar and Spalding, 1972). Central differencing was used for both the convection and diffusion terms.

The set of nonlinear, coupled discrete equations was iteratively satisfied by a segregated multigrid procedure in which all the equations were cycled up and down several levels of coarse grids. The central concept in the multigrid procedure is that on any grid, the high frequency, oscillatory errors are fast to converge but the smooth, low-frequency errors take a considerably large number of iterations to be annihilated. Transferring these low-frequency errors to coarser grids accelerates their convergence and produces a grid-independent rate of convergence. [For more details on the multigrid procedure, see Trottenberg et al. (2001).] The velocity field is converged to a high accuracy with the sum of absolute mass residuals over the duct cross section reduced to 10^{-6} of the inlet mass flow rate. The scalar concentration was also discretized by central differences with a finite-volume procedure and solved by marching in the streamwise direction with fixed increments of the angular coordinate. However, unlike the momentum and continuity equations, the scalar transport equation is solved by a single-grid procedure because of the large diagonal term arising from the upstream convection term.

Results

Grid-sensitivity tests

The computer program was first validated in a number of model problems, such as the flow in a driven cavity, natural convection in a square enclosure, and flow in a channel. It was then applied to the present problem of flow in a curved square duct. The fully developed flow solutions at high Reynolds numbers were first compared with previous results (Ghia and Sokhey, 1977; Thangam and Hur, 1990) to validate the implementation of the curvature terms. After this extensive validation, grid-sensitivity tests were done for the present Reynolds numbers with three grids consisting of 32 × 32, 64 × 64, and 128 × 128 uniformly spaced control volumes. Figure 3 shows the profiles of the cross-stream velocities at Re = 20 and R_c (= R/d) = 2.5 for the three grids. It is clear from these plots that the 64 × 64 grid gave good accuracy, given that the velocity profiles agreed closely with the solution on the 128 × 128 grid. For the scalar field, grid independence was more difficult when the Schmidt number was high. As a result, much higher resolutions were needed for grid-independent mixing efficiencies. A systematic grid sensitivity investigation was performed at Sc = 1000 and Re = 20, with grids as fine as 640 × 640 control volumes for a curved channel of radius ratio (R/d) of 2.5. Figure 4 shows the unmixedness coefficient (η, defined by Eq. 9) as a function of streamwise distance for different grids. It can be seen that a 512 × 512 grid was necessary to obtain grid-independent results at Sc = 1000. Sensitivity tests were also performed on the forward step for the scalar field computations. A forward step size of 0.1 degree was found adequate for the finest cross-stream grid.

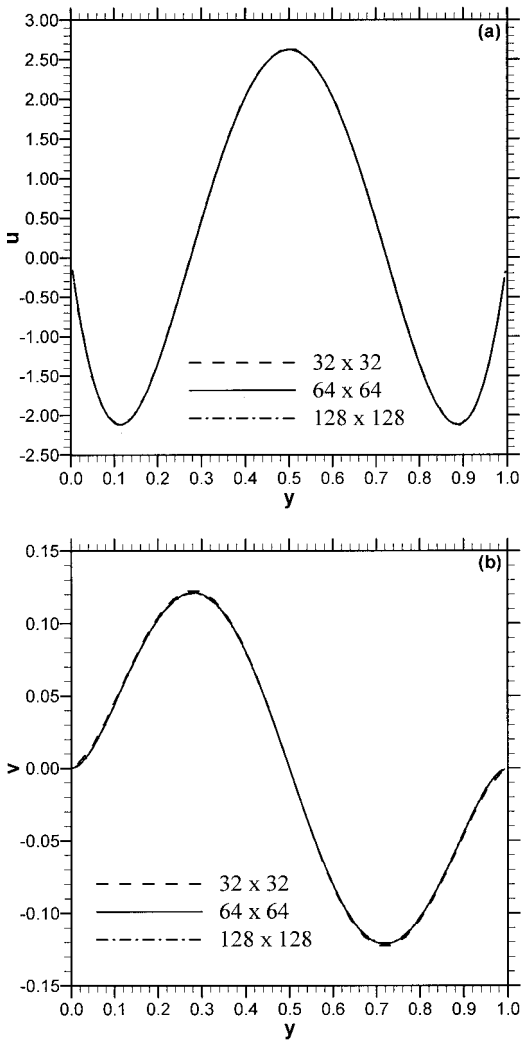

Figure 3. Profiles of the cross-stream velocities in the curved duct (Re = 20 and R_c = 2.5) for three grids.

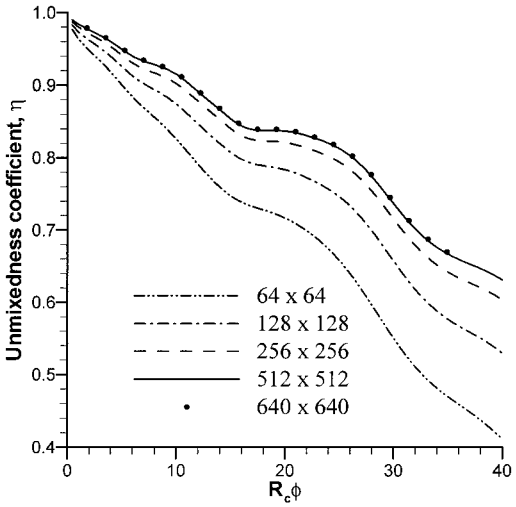

Figure 4. Unmixedness coefficient as a function of streamwise distance for different grids (Re = 20, R_c = 2.5, and Sc = 1000).

Straight duct

Before proceeding to the case of a curved duct, we first computed the mixing effectiveness of a straight duct of square cross section. The nondimensional velocity distribution in a straight duct is given by the solution to the equation

$$\frac{\partial^2 w}{\partial x^2} + \frac{\partial^2 w}{\partial y^2} = \frac{1}{\mathrm{Re}} \frac{dp}{dz} \tag{7}$$

where z is the nondimensional streamwise distance; x and y are the nondimensional coordinates (nondimensionalized with duct dimension d) in the cross-stream directions; dp/dz is a nondimensional pressure gradient; and Re is the Reynolds number. For this equation, a series solution (Bird et al., 1960) is available. The concentration equation simplifies to

$$\frac{\partial (wc)}{\partial z} = \frac{1}{\mathrm{Re} \cdot \mathrm{Sc}} \left(\frac{\partial^2 c}{\partial x^2} + \frac{\partial^2 c}{\partial y^2} \right) \tag{8}$$

Because the fully developed nondimensional velocity profile is invariant with the Reynolds number, the concentration dis-

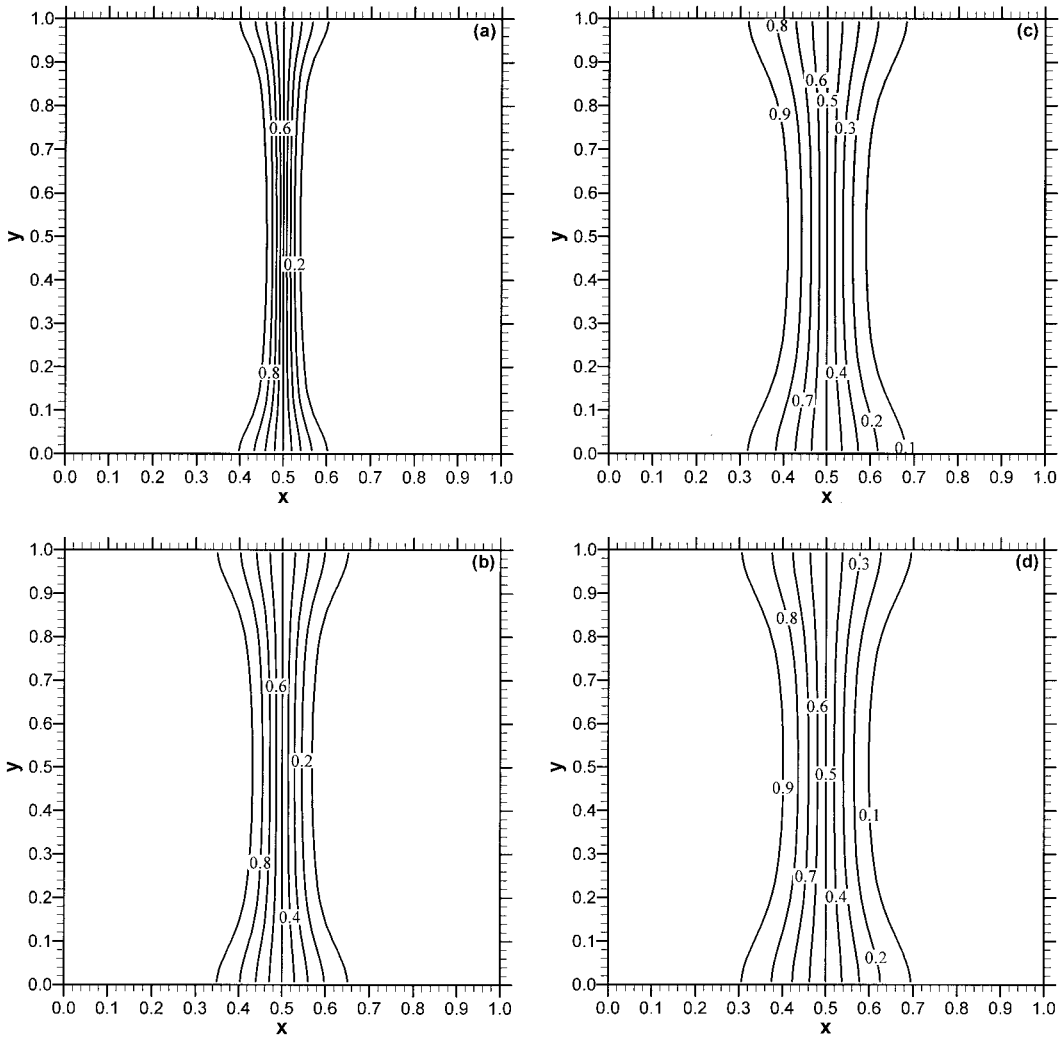

Figure 5. Distribution of the scalar concentration in a straight duct for a value of Re · Sc = 10^4 at (a) z = 10, (b) z = 30, (c) z = 50, and (d) z = 60.

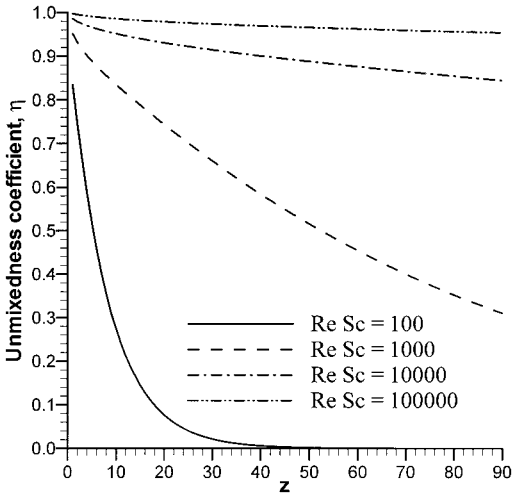

Figure 6. Unmixedness coefficient as a function of distance along a straight duct.

tribution is a function of only the product of Reynolds number (Re) and the Schmidt number (Sc). We have computed the spatial distribution of $c(x, y, z)$ and defined a unmixedness coefficient as

$$\eta = \frac{\left\{\dfrac{\int\int [c(x, y, z) - \bar{c})]^2 dxdy}{\int\int dxdy}\right\}^{1/2}}{\bar{c}} \tag{9}$$

where η is a unmixedness coefficient and dx, dy are sizes of control volumes in the x and y directions, respectively. The quantity $\bar{c}$ represents a local flow weighted mean concentration over the cross section given by

$$\bar{c} = \frac{\int\int w(x, y)c(x, y, z)dxdy}{\int\int w(x, y)dxdy} \tag{10}$$

Figure 5 shows the distribution of the scalar concentration in the duct cross section at several planes, for a value of Re · Sc =

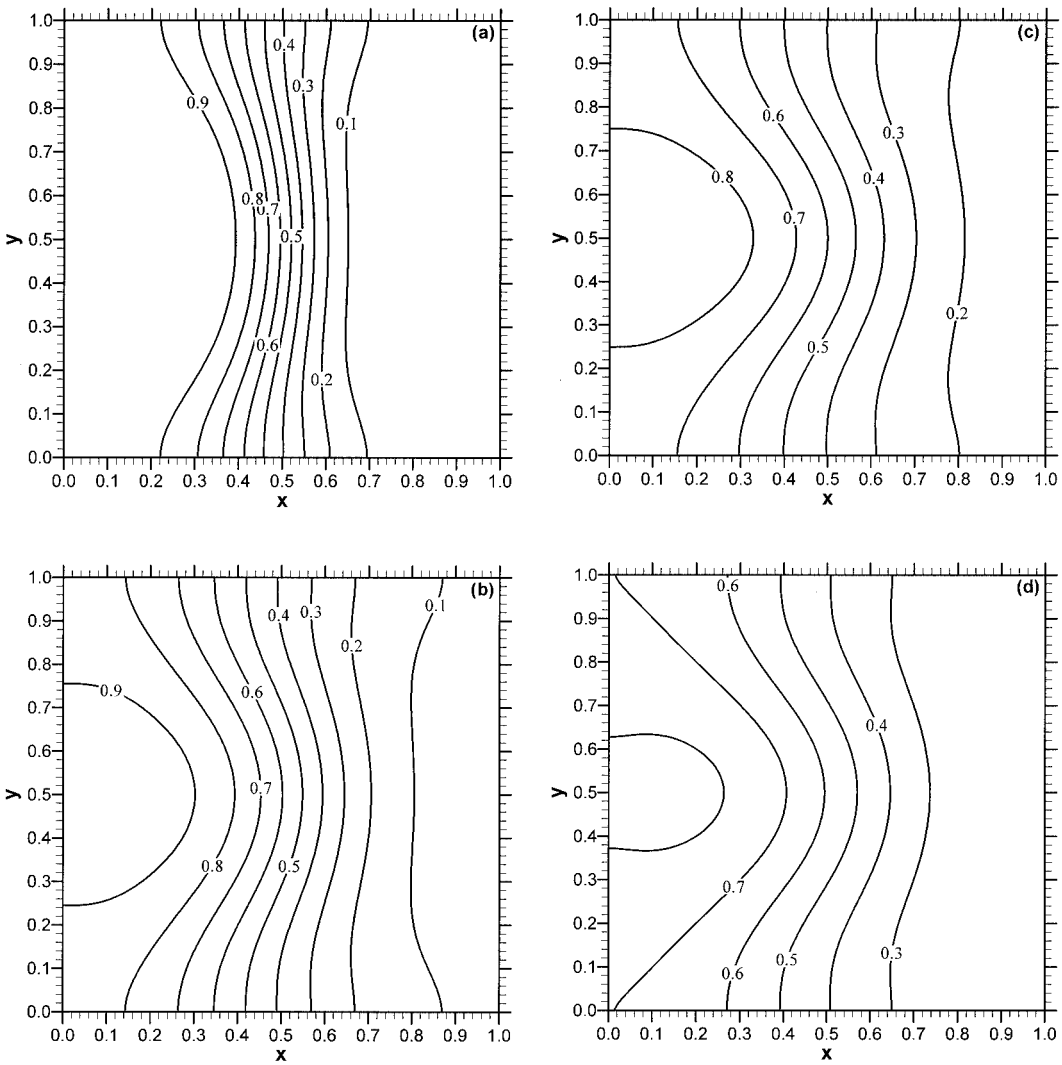

Figure 7. Distribution of the scalar concentration in the curved duct for Reynolds number of 1.0, Schmidt number of 1000, and R_c of 3.5 at (a) $R_c\phi$ = 10, (b) $R_c\phi$ = 30, (c) $R_c\phi$ = 50, and (d) $R_c\phi$ = 60.

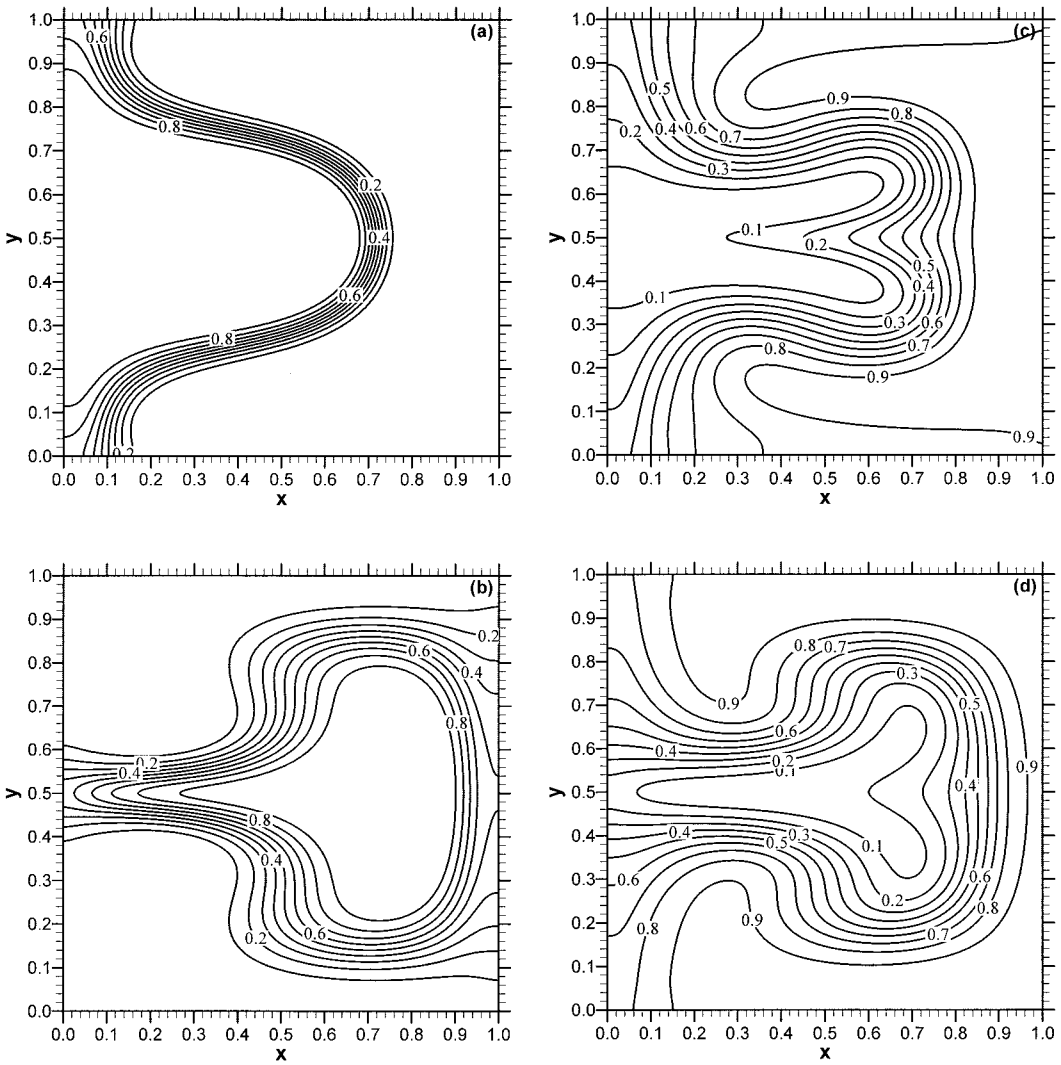

Figure 8. Distribution of the scalar concentration in the curved duct for Reynolds number of 10, Schmidt number of 1000, and R_c of 3.5 at (a) $R_c\phi = 10$, (b) $R_c\phi = 30$, (c) $R_c\phi = 50$, and (d) $R_c\phi = 60$.

10^4. This corresponds to a liquid with a Schmidt number of 1000 and a flow Reynolds number of 10. It can be seen that for this small Reynolds number the mixing is very poor, as seen by only a small spread of the concentration contours. The relatively larger diffusion near the duct walls arises from the slower axial velocity in that region. We computed η for a number of values of (Re · Sc) as a function of distance along the duct. This is shown in Figure 6. It can be seen that the unmixedness coefficient increases ($\eta \approx 1.0$) as the product (Re · Sc) is increased. Because the mixing is attributed only to molecular diffusion and no cross-stream velocities are present, increasing Sc decreases the scalar diffusivity and thus the mixing efficiency.

Curved duct

We next studied the mixing efficiency in a curved duct with different parameters. Unlike mixing in a hydrodynamically fully developed straight-duct flow, where the mixing is governed by a single parameter (Re · Sc), in a curved duct the mixing is more complex because of the curvature-induced secondary flows that depend on the Reynolds number and the curvature ratio. Thus the extent of mixing is a complex function of the Reynolds number, duct curvature, and the molecular diffusion coefficient. The relative effectiveness of a curved duct over a straight duct is therefore quite complex and intriguing.

Figure 7 shows the mixing behavior in a curved channel ($R_c = 3.5$) through cross-sectional distributions of the concentration at several streamwise distances for a Reynolds number of 1.0 and Schmidt number of 1000. At the inlet, the concentration is unity in the left vertical half of the duct and zero in the right half. The Dean vortices are from the left to the right of the cross section and the flow is symmetrical over the horizontal midplane (Figure 1). It can be seen that the effect of the Dean vortices is to bend the concentration contours and mix the two halves through advection of the concentration. However, at Re = 1.0, the Dean vortices are relatively weak and the mixing ascribed to secondary flow is not significant. When the Reynolds number is increased to 10, the mixing attributed to the secondary flow is much stronger, as seen in Figure 8. The

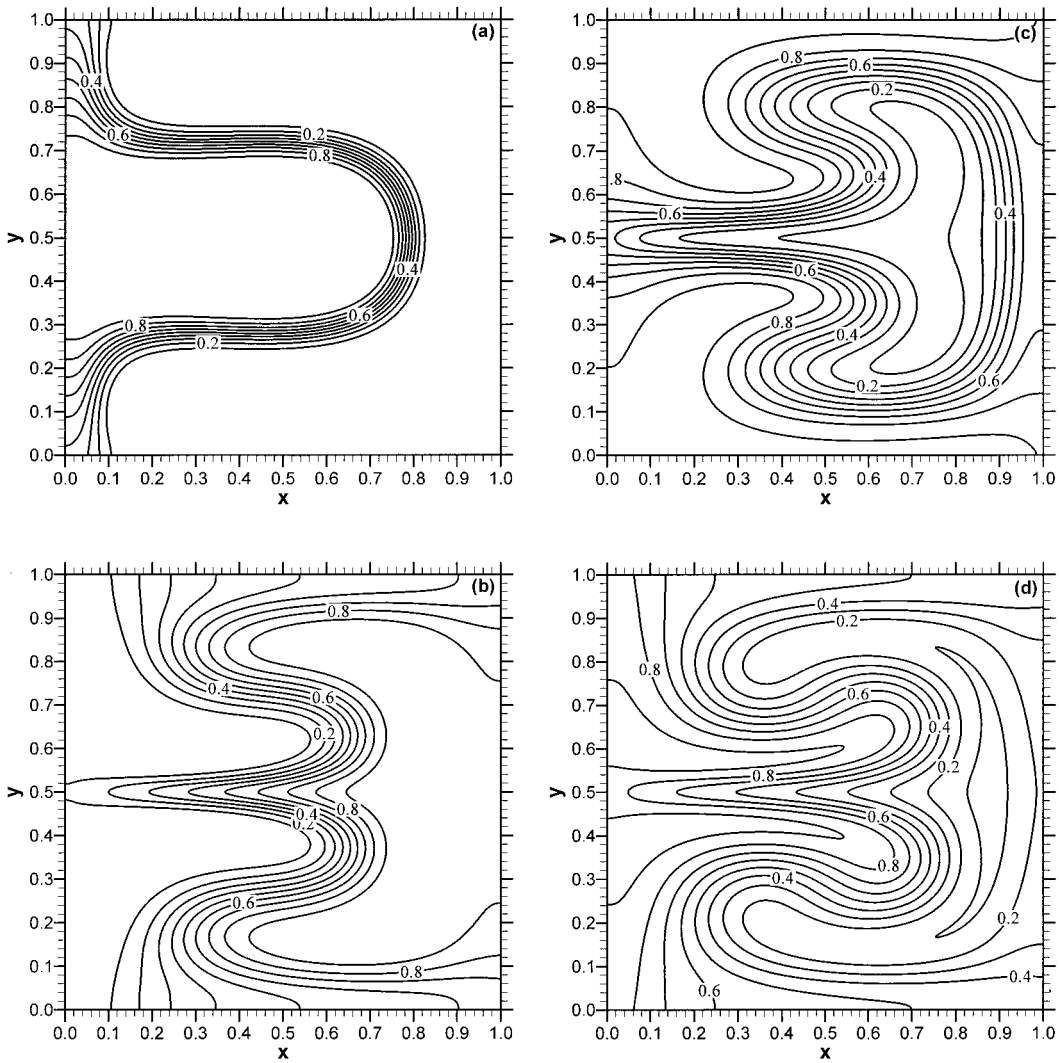

Figure 9. Distribution of the scalar concentration in the curved duct for Reynolds number of 10, Schmidt number of 1000, and R_c of 2.5 at (a) $R_c\phi = 10$, (b) $R_c\phi = 30$, (c) $R_c\phi = 50$, and (d) $R_c\phi = 60$.

contours of concentration are much more twisted by the secondary flow, resulting in enhanced surface area for diffusion and mixing. When the radius of curvature is decreased to 2.5, the secondary flow intensifies and the mixing further enhances. Figure 9 shows contours of concentration for Re = 10, Sc = 1000, and $R_c = 2.5$.

A summary of a number of calculations is shown in Figure 10, which plots the unmixedness coefficient (given by Eq. 9) against streamwise distance for several combinations of Re and Sc and for a radius ratio of 3.5. The corresponding figure for $R_c = 2.5$ is given in Figure 11. We first see that when Re = 0.1, the residence time in the duct is large and mixing occurs primarily by molecular diffusion. The secondary flow is small and the mixing efficiency in a curved duct is much the same as that in a straight duct. The mixing at Sc = 100 is obviously faster than that at Sc = 1000. Also, it can be seen that the curves for Sc = 100, Re = 1.0 and Sc = 1000, Re = 0.1 are nearly the same. This implies that the effect of Dean vortices is small at Re = 1.0, and because the product of (Re · Sc) is the same, the mixing is primarily diffusion driven.

As the Reynolds number is increased and Sc is fixed at 100, the mixing efficiency decreases from that at Re = 1.0. This is because the residence time is decreased and the mixing arising from diffusion decreases. The coefficient of unmixedness η is larger at Re = 10, although the curvature-induced secondary flow is larger than that at Re = 1.0. However, when the Schmidt number is increased to 1000, implying very small diffusion coefficient, the effect of the Reynolds number (Re increasing from 10 to 20) is to improve mixing. At Sc = 1000 and Re = 1.0, the product of Re and Sc is smaller than that at Re = 10, and therefore the diffusion mixing is greater. Thus, the extent of mixing depends not only on the product of Re and Sc but also on Re and the duct curvature. The balance of these convection and diffusion processes eventually governs the overall cross-sectional averaged mixing coefficient.

Figure 11, although similar to Figure 10, shows the effects of slightly stronger Dean vortices attributed to the smaller radius of curvature. The intensity of secondary flow depends on the Dean number, defined as $De = Re\sqrt{d/R_c}$. Figure 12 shows the maximum secondary flow in the center of the duct, normalized

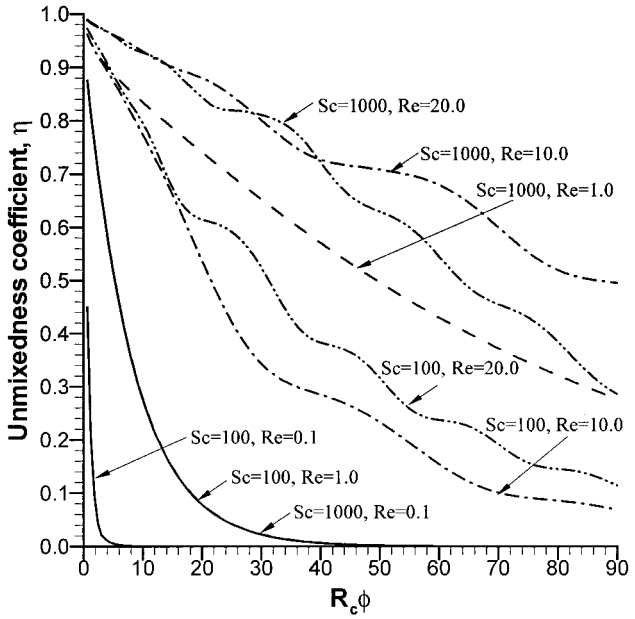

Figure 10. Unmixedness coefficient as a function of distance along the curved duct (R_c = 3.5).

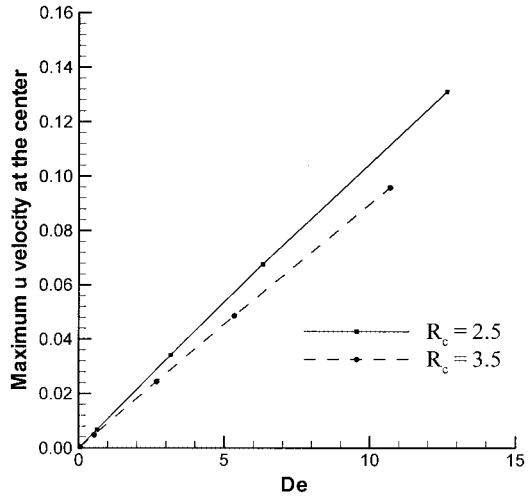

Figure 12. Normalized maximum secondary flow velocity in the center of the curved duct as a function of the Dean number.

by the average streamwise velocity, as a function of the Dean number. It can be seen that in this range of Dean numbers, the secondary flow increases linearly with the Dean number. The increased Dean number increases the secondary flow and thus the mixing efficiency.

Conclusions

It can be seen that a curved channel, whether of constant or varying curvature, is far more efficient in mixing than a straight channel of similar length when moderate Reynolds numbers are considered. The important aspect is that mixing in curved channels is significantly greater at higher Reynolds numbers, whereas in straight channels, mixing efficiency decreases when the Reynolds number increases. The advantage of a curved channel is that it has a small footprint area and is also easy to fabricate, compared to other active and passive geometries presented in the literature. In a curved channel, the increase in Reynolds number produces increased levels of secondary flow, which produce enhanced mixing. In contrast, the increase in Reynolds number in a straight channel decreases the residence time for diffusion to take place, and thus the mixing efficiency diminishes. At low Reynolds numbers, of the order of 0.1, a curved channel is not very attractive as a mixer because of the low intensity of the secondary flow. In such a case other means of convective mixing, such as buoyancy-driven flows or electrokinetic flows, should be considered. Alternately, the mixing surface area can be increased by segmenting the inflow streams into alternating layers of the two different fluids. Such lamination was previously considered in Branebjerg et al. (1996). However, for a curved channel, it is sufficient to implement the lamination only at the inlet of the channel. With lamination, the surface area for diffusion is considerably increased, resulting in enhanced mixing.

A more compact design—in which the mixer is made in one plane with curved channels of either spiral shape or embedded within each other—can also be developed. In such a channel, the radius of curvature varies either continuously (spiral) or in sudden steps of one duct height. Recent experiments in such geometries (Vanka et al., 2003) revealed that mixing enhancement similar to that presented above can be obtained. Such planar configurations can be incorporated into micro total analysis systems.

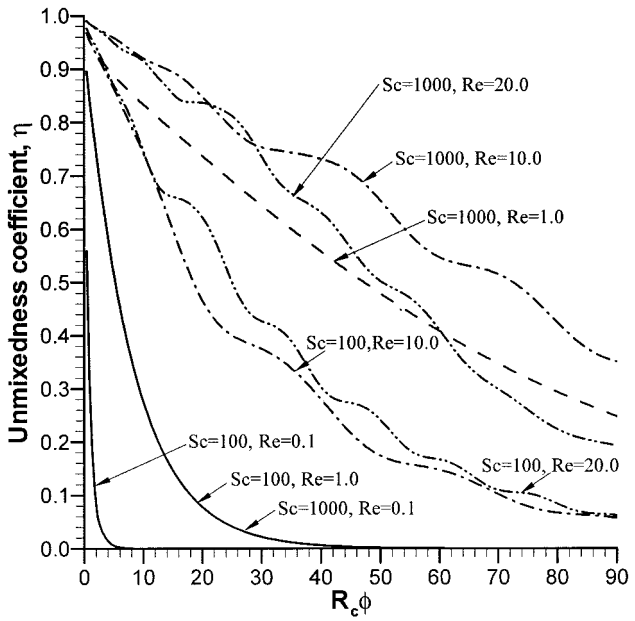

Figure 11. Unmixedness coefficient as a function of distance along the curved duct (R_c = 2.5).

Literature Cited

Aref, H., "Stirring by Chaotic Advection," *J. Fluid Mech.*, **143**, 1 (1984).
Berger, S. A., L. Talbot, and L. S. Yao, "Flow in Curved Pipes," *Ann. Rev. Fluid Mech.*, **15**, 461 (1983).
Bird, R. B., W. E. Stewart, and E. Lightfoot, *Transport Phenomena*, Wiley, New York (1960).

Branebjerg, J., P. Graveson, J. P. Krog, and C. R. Nielsen, "Fast Mixing by Lamination," MEMS 96, San Diego, CA, pp. 441–446 (1996).
Brody, J. P., P. Yager, R. E. Goldstein, and R. H. Austin, "Biotechnology at Low Reynolds Numbers," *Biophys. J.*, **71**, 3430 (1996).
Dean, W. R., "Note on the Motion of Fluid in a Curved Pipe," *Philos. Mag.*, **4**, 208 (1927).
Deshmukh, A. A., D. Liepman, and A. P. Pisano, "Continuous Micromixer with Pulsatile Micropumps," Proc. of Solid-State Sensor & Actuator Workshop, Hilton Head, SC, June 4–8 (2000).
Evans, J., D. Liepmann, and A. P. Pisano, "Planar Laminar Mixer," Proc. of the IEEE 10th Annual Workshop of MEMS Workshop, Nagoya, Japan, pp. 96–101 (1997).
Ghia, K. N., and J. S. Sokhey, "Laminar Incompressible Viscous Flow in Curved Ducts of Regular Cross-Sections," *ASME J. Fluids Eng.*, **99**, 640 (1977).
Gravesen, P., J. Branejberg, and O. S. Jensen, "Microfluidics—A Review," *J. Micromech. Microeng.*, **3**, 168 (1993).
Jensen, K., "Microreaction Engineering—Is Small Better?," *Chem. Eng. Sci.*, **56**, 293 (2001).
Jones, S. W., O. M. Thomas, and H. Aref, "Chaotic Advection by Laminar Flow in a Twisted Pipe," *J. Fluid Mech.*, **209**, 335 (1989).
Lee, Y. K., J. Deval, P. Tabeling, and C.-M. Ho, "Chaotic Mixing in Electrokinetically and Pressure Driven Micro Flows," Proc. of the 14th IEEE Workshop on MEMS, Interlaken, Switzerland, pp. 483–486 (2001).
Lee, Y. K., P. Tabeling, C. Shih, and C.-M. Ho, "Characterization of a MEMS-Fabricated Mixing Device," Proc. of MEMS, ASME, IMECE Conf., pp. 505–511 (2000).
Liu, R. H., M. A. Stremler, K. V. Sharp, M. G. Olsen, J. G. Santiago, R. J. Adrian, H. Aref, and D. J. Beebe, "Passive Mixing in a Three-Dimensional Serpentine Microchannel," *JMEMS*, **9**(2), 190 (2000).
Miyake, R., T. S. J. Lammerink, M. Elwenspoek, J. H. J. Fluitman, "Micro Mixer with Fast Diffusion," MEMS-93, Fort Lauderdale, FL, (Feb. 1993).
Patankar, S. V., and D. B. Spalding, "A Calculation Procedure for Heat, Mass and Momentum Transfer in Three-Dimensional Parabolic Flows," *Int. J. Heat Mass Transfer*, **15**, 1787 (1972).
Pratap, V. S., and D. B. Spalding, "Numerical Computations of the Flow in Curved Ducts," *Aero. Q.*, **26**, 219 (1975).
Thangam, S., and N. Hur, "Laminar Secondary Flows in Curved Rectangular Ducts," *J. Fluid Mech.*, **217**, 421 (1990).
Trottenberg, U., C. W. Oosterlee, and A. Schuller, *Multigrid*, Academic Press, San Diego, CA (2001).
Vanka, S. P., C. M. Winkler, J. Coffman, E. Linderman, S. Mahjub, and B. Young, "Novel Low Reynolds Number Mixers for Microfluidic Applications," ASME/JSME Joint Fluids Engineering Summer Conference, Hawaii, July 5–9 (2003).
Volpert, M., C. D. Meinhart, I. Mezic, and M. Dahleh, "An Actively Controlled Micromixer," Proc. of MEMS, ASME, IMECE Conf., Nashville, TN, pp. 483–487 (1999).
Yi, M., and H. H. Bau, "The Kinematics of Bend-Induced Stirring by Micro-Conduits," Proc. of MEMS, ASME, IMECE Conf., Vol. 2, pp. 489–496 (2000).
Yi, M., H. H. Bau, and H. Hu, "A Peristaltic Meso-Scale Mixer," Proc. of MEMS, ASME, IMECE Conf., pp. 367–374 (2000).

Manuscript received Sep. 9, 2003, and revision received Jan. 12, 2004.